

Deeply Virtual Compton Scattering on nucleons and nuclei in generalized vector meson dominance model

K. Goeke,^{1,*} V. Guzey,^{2,†} and M. Siddikov^{1,3,‡}

¹*Institut für Theoretische Physik II,*

Ruhr-Universität-Bochum, D-44780 Bochum, Germany

²*Theory Center, Jefferson Lab, Newport News, VA 23606, USA*

³*Theoretical Physics Dept, Uzbekistan National University, Tashkent 700174, Uzbekistan*

Abstract

We consider Deeply Virtual Compton Scattering (DVCS) on nucleons and nuclei in the framework of generalized vector meson dominance (GVMD) model. We demonstrate that the GVMD model provides a good description of the HERA data on the dependence of the proton DVCS cross section on Q^2 , W (at $Q^2 = 4 \text{ GeV}^2$) and t . At $Q^2 = 8 \text{ GeV}^2$, the soft W -behavior of the GVMD model somewhat underestimates the W -dependence of the DVCS cross section due to the hard contribution not present in the GVMD model. We estimate $1/Q^2$ power-suppressed corrections to the DVCS amplitude and the DVCS cross section and find them large. We also make predictions for the nuclear DVCS amplitude and cross section in the kinematics of the future Electron-Ion Collider. We predict significant nuclear shadowing, which matches well predictions of the leading-twist nuclear shadowing in DIS on nuclei.

PACS numbers: 12.40.Vv, 13.60.Hb, 25.30.Rw

*Electronic address: Klaus.Goeke@tp2.rub.de

†Electronic address: vguzey@jlab.org

‡Electronic address: Marat.Siddikov@tp2.rub.de

I. INTRODUCTION

During the last decade, one of main focuses of hadronic physics has been the study of the hadronic structure using hard exclusive reactions, such as Deeply Virtual Compton Scattering (DVCS), $\gamma^*N \rightarrow \gamma N$, and hard exclusive meson production (HEMP), $\gamma^*N \rightarrow MN$. These processes have been the subject of intensive theoretical and experimental investigations [1, 2, 3, 4, 5, 6, 7, 8, 9, 10, 11, 12, 13, 14]. In addition, there were investigated "inverse" hard exclusive reactions such as $\gamma N \rightarrow \gamma^*N \rightarrow l^+l^-N$ [15] and $\pi N \rightarrow \gamma^*N \rightarrow l^+l^-N$ [16], and "u-channel" reactions such as $\gamma^*\gamma \rightarrow \pi\pi$ [17].

The interest to the DVCS and HEMP reactions is motivated by the fact that in the Bjorken limit (large Q^2), the corresponding amplitudes factorize [7, 8] in convolution of perturbative (hard) coefficient functions with nonperturbative (soft) matrix elements, which are parameterized in terms of generalized parton distributions (GPDs). GPDs are universal (process-independent) functions that contain information on parton distributions, form factors and correlations in hadrons. GPDs also parameterize parton correlations in matrix elements describing transitions between two different hadrons, which appear in reactions such as e.g. $\gamma^*p \rightarrow \pi^+n$ [18, 19].

While the description of DVCS and HEMP based on the factorization approach is most general, in experiments the values of the virtualities Q^2 are below the range required for the validity of the factorization theorem [20, 21, 22, 23, 24, 25]. Hence, contributions of higher-twist effects might be substantial (it is an open issue how large these effects are), which will affect the extraction of GPDs from the data. Therefore, it is important to have an effective model for the DVCS and HEMP amplitudes, which would interpolate between the photoproduction ($Q^2 \approx 0$) and deep inelastic ($Q^2 \sim \mathcal{O}(10) \text{ GeV}^2$) regimes.

In this paper, using the generalized vector meson dominance (GVMD) model [26, 27, 28], which is consistent with perturbative QCD at small transverse distances [29], we derive expressions for the amplitudes of DVCS on nucleons and nuclei, which are valid at high energies and which are applicable over a wide range of Q^2 . We show that the resulting cross section of DVCS on nucleons compares well to the HERA data [30, 31]. In particular, the dependence of the DVCS cross section on Q^2 , W (at $Q^2=4 \text{ GeV}^2$) and t are reproduced rather well; the W -dependence of the cross section at $Q^2=8 \text{ GeV}^2$ is somewhat underestimated, which can be interpreted as due to the onset of the hard regime beyond the soft dynamics

of the GVMD model.

We also estimate the relative contribution of $1/Q^2$ -corrections, which correspond to the higher-twist corrections in perturbative QCD [32, 33, 34]. We show that these corrections are large: the contribution of the $1/Q^2$ -corrections to the DVCS amplitude at $t = t_{\min}$ is 20% at $Q^2 = 2 \text{ GeV}^2$, 11% at $Q^2 = 4 \text{ GeV}^2$ and 6% at $Q^2 = 8 \text{ GeV}^2$; the contribution of the $1/Q^2$ -corrections to the t -integrated DVCS cross section is 56% at $Q^2 = 2 \text{ GeV}^2$, 32% at $Q^2 = 4 \text{ GeV}^2$ and 17% at $Q^2 = 8 \text{ GeV}^2$.

We also make predictions for the DVCS cross section on nuclear targets, which are relevant for the physics program of the future Electron-Ion Collider. We predict significant nuclear shadowing, which matches well predictions of the leading-twist nuclear shadowing in DIS on nuclei [35].

The hypothesis of vector meson dominance (VMD) [36] assumes a definite relation between the amplitude of the photon (real or virtual)-hadron interaction, $\mathcal{A}(\gamma_{\text{tr}}^* + T \rightarrow \dots)$, and a linear combination of the amplitudes of the corresponding strong production by transversely polarized vector mesons, $\mathcal{A}(V_{\text{tr}} + T \rightarrow \dots)$,

$$\mathcal{A}(\gamma_{\text{tr}}^* + T \rightarrow \dots) = \sum_{V=\rho,\omega,\phi} \frac{e}{f_V} \frac{m_V^2}{m_V^2 + Q^2} \mathcal{A}(V_{\text{tr}} + T \rightarrow \dots), \quad (1)$$

where f_V is the coupling constant determined from the $V \rightarrow e^+e^-$ decay; m_V is the vector meson mass; Q^2 is the virtuality of the photon; T denotes any hadronic target. Note that Eq. (1) is written for the transversely polarized photons. In Eq. (1), we took into account only the contribution of the ρ^0 , ω and ϕ mesons.

The VMD model and its generalizations explain a large wealth of data on the real and virtual ($Q^2 < 1 \text{ GeV}^2$) photon-hadron scattering, which include the pion electric form factor, total cross sections of photon-nucleon and photon-nucleus scattering (inclusive structure functions), exclusive production of vector mesons on nucleons and nuclei, exclusive production of pseudoscalar mesons, for a review, see [37].

As the virtuality of the photon increases, $Q^2 > 1 \text{ GeV}^2$, the simple VMD model, see Eq. (1), becomes inadequate since it leads to the violation of the approximate Bjorken scaling. In order to restore the approximate Bjorken scaling, the simple VMD model can be generalized [38]. This can be done using the model-independent method of mass-dispersion representation for the virtual photon-hadron scattering amplitude [39].

In order to illustrate the approach, let us consider the forward virtual photon-hadron

scattering amplitude. The dispersion representation for the imaginary part of $\mathcal{A}(\gamma_{\text{tr}}^* + T \rightarrow \gamma_{\text{tr}}^* + T)$ reads

$$\Im m \mathcal{A}(\gamma_{\text{tr}}^* + T \rightarrow \gamma_{\text{tr}}^* + T)|_{t=0} = \int \frac{dM^2 M^2}{M^2 + Q^2} \frac{dM'^2 M'^2}{M'^2 + Q^2} \frac{e}{f_V} \sigma_{VV'} \frac{e}{f_{V'}}, \quad (2)$$

where $\sigma_{VV'}$ is the $V + T \rightarrow V' + T$ scattering cross section (spectral function) which weakly depends on the masses M and M' . The main idea of the GVMD model [26, 27, 28] is to approximate Eq. (2) by an infinite series of (fictitious) vector mesons of ever increasing mass, allowing for both diagonal ($V + T \rightarrow V + T$) and non-diagonal ($V + T \rightarrow V' + T$) transitions. The role of the non-diagonal transitions is to partially cancel the diagonal transitions so that, effectively, $\sigma_{VV'} \propto 1/M^2$ for large M^2 . This softens the spectral function and leads to the approximate Bjorken scaling of the inclusive structure function $F_2(x, Q^2)$, see [29] for the discussion.

In the language of the color dipole model, the fact that $\sigma_{VV'} \propto 1/M^2$ for large M^2 means that besides dipoles of large transverse sizes, the virtual photon also contains small transverse-size dipoles. The latter fact is called color transparency.

One should note that, while the simple vector meson dominance model fails to reproduce the approximate scaling of the *inclusive* structure function $F_2(x, Q^2)$ (see above), the simple VMD model predicts the correct Q^2 -behavior of cross sections of *exclusive* reactions, such as $\gamma^* p \rightarrow \pi^+ n$ [40, 41]. This is also true for DVCS: Even the simple VMD model provides the correct Q^2 -behavior of the DVCS cross section (up to logarithmic corrections).

The structure of this paper is the following. In Sect. II, we explain main assumptions of the GVMD model, which we further generalize to take into account a non-zero momentum transfer $t \neq 0$. We derive the expression for the amplitude of DVCS on the nucleon and make predictions for the DVCS cross section. We demonstrate that the GVMD model provides a good description of the HERA data on the W , Q^2 and t -dependence of the cross section of DVCS on the proton [30, 31]. In this section, we also estimate $1/Q^2$ -corrections to the DVCS amplitude and the DVCS cross section. Predictions for the nuclear DVCS amplitude and for the cross section of DVCS on nuclei in the collider kinematics are presented in Sect. III. In Sect. IV, we summarize and discuss our results.

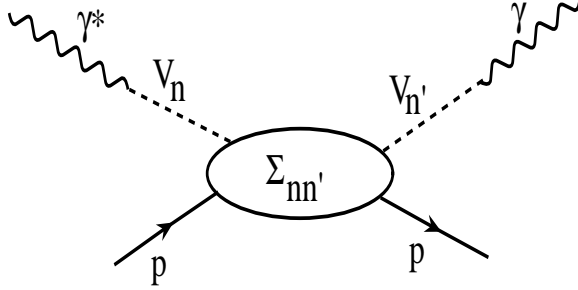


FIG. 1: The DVCS amplitude in the GVMD model, see Eq. (3).

II. DVCS ON THE NUCLEON

In this section, we extend the generalized vector meson dominance (GVMD) model [26, 27, 28] to the off-forward case and apply it to Deeply Virtual Compton Scattering (DVCS) on the nucleon.

A. DVCS amplitude

The GVMD model assumes that the virtual (real) photon interacts with the hadronic target by fluctuating into a coherent and infinite sum of fictitious vector mesons V_n . Then, the DVCS amplitude at the photon level, $\mathcal{A}(\gamma^* p \rightarrow \gamma p)$, can be graphically presented as depicted in Fig. 1.

In the GVMD model, the DVCS amplitude for transversely polarized virtual photons reads

$$\mathcal{A}(\gamma_{\text{tr}}^* + p \rightarrow \gamma + p) = \sum_{n,n'=0}^{\infty} \frac{e}{f_n} \frac{M_n^2}{M_n^2 + Q^2} \Sigma_{n,n'}(W, t) \frac{e}{f_{n'}}, \quad (3)$$

where $W^2 = (p_{\gamma^*} + p)^2$ with p_{γ^*} the momentum of the initial photon and p the momentum of the initial proton; $t = (p' - p)^2$ with p' the momentum of the final proton. The masses

M_n and the coupling constants f_n are connected by the following relations,

$$\frac{M_n^2}{M_0^2} = \frac{f_n^2}{f_0^2} = (1 + 2n), \quad (4)$$

where $M_0 = m_\rho$ and $f_0 = f_\rho$ refer to the physical ρ^0 meson.

Note that the relation of the vector mesons V_n conventionally used in the GVMD model to physical $J^P = 1^-$ vector mesons found in the Review of particle physics [42] is not direct. The motivation for this is that while the vector meson masses are known with a reasonable accuracy up to $M_\rho \gtrsim 2$ GeV, there is no accurate data on the partial decay width $\Gamma_{e^+e^-}$ for mesons heavier than $\rho(1450)$. On the other hand, the parameterization (4) provides reasonable results for physical observables. One can check that the linear n -dependence of the ratio M_n^2/M_0^2 in Eq. (4) is confirmed experimentally for large- n [42]. However, the slope of the n -dependence is underestimated by approximately a factor of two.

It is important to point out that, at high energies, the DVCS cross section at the photon level is dominated by the contribution of the transversely polarized virtual photons due to the helicity conservation [31]. In the language of the color dipole model, this dominance is explained by the dominance of the large transverse-size dipoles over the small transverse-size dipoles, see [13] for the discussion. Therefore, Eq. (3) gives the complete description of the DVCS amplitude.

The quantity $\Sigma_{n,n'}(t)$ is the $V_{n,\text{tr}} + p \rightarrow V_{n',\text{tr}} + p$ scattering amplitude, see Fig. 1. The matrix $\Sigma_{n,n'}(t)$ is assumed to have a tri-diagonal form with the following non-zero elements,

$$\begin{aligned} \Sigma_{n,n}(W, t) &= i\sigma_{\rho p}(W^2)(1 - i\eta)F_n(t), \\ \Sigma_{n,n+1}(W, t) &= \Sigma_{n+1,n}(W, t) = -\frac{1}{2} \frac{M_n}{M_{n+1}} \left(1 - 2\delta \frac{m_\rho^2}{M_n^2}\right) \Sigma_{n,n}(W, t), \end{aligned} \quad (5)$$

where $\sigma_{\rho p}$ is the ρ meson-proton cross section for the transversely polarized meson; η is the ratio of the real to imaginary parts of the ρ meson-proton scattering amplitude; $\delta = 0.2$ is the parameter of the model.

The function $F_n(t)$ models the t -dependence of $\Sigma_{n,n'}(t)$, which goes beyond the original formulation of the GVMD model [26, 27, 28], which addressed only the forward $t = 0$ limit. In our analysis, we use the following form of $F_n(t)$,

$$F_n(t) = \exp \left(-\frac{1}{2} \left[\frac{1}{n+1} B_1 + \frac{n}{n+1} B_2 \right] |t| \right), \quad (6)$$

where $B_1 = 11 \text{ GeV}^{-2}$ and $B_2 = 4.3 \text{ GeV}^{-2}$. The choice of the slopes B_1 and B_2 is motivated as follows.

For the moment, let us replace the final real photon by the ρ meson. In the photoproduction limit, the $\gamma p \rightarrow \rho p$ cross section measured at HERA by the H1 collaboration was fitted to the form $\exp(-B|t|)$ with the slope $B = (10.9 \pm 2.4 \pm 1.1) \text{ GeV}^{-2}$ [43]. The ZEUS measurement gives essentially the same value of B [44].

In electroproduction, the slope of the exponential fit to the $\gamma^* p \rightarrow \rho p$ cross section is much smaller than in photoproduction: It decreases from $B = (8.0 \pm 0.5 \pm 0.6) \text{ GeV}^{-2}$ at $Q^2 = 1.8 \text{ GeV}^2$ to $B = (4.7 \pm 1.0 \pm 0.7) \text{ GeV}^{-2}$ at $Q^2 = 21.2 \text{ GeV}^2$ [45].

This decrease of the slope of the t -dependence with increasing Q^2 is effectively parameterized by Eq. (6) as a decrease of the slope with the increasing number of the vector meson n . Indeed, close to the photoproduction limit, the dominant contribution to the sum in Eq. (3) comes from the $n = 0$ term. In the opposite limit of large Q^2 , terms with large n , up to $M_n^2 \sim Q^2$, contribute to the sum. Choosing $Q^2 = 0$ and $Q^2 = 21.2 \text{ GeV}^2$ as reference points, we determine the values of the slopes B_1 and B_2 in Eq. (6).

It is clear from the above discussion that while the value of the slope B_1 in Eq. (6) is model-independent, the value of the slope B_2 is somewhat more uncertain. We have chosen not to introduce Q^2 -dependent slopes B_1 and B_2 since this would contradict the spirit of the VMD model: The W and t -dependence of the DVCS amplitude is determined solely by the vector meson-proton scattering amplitudes; the vector meson propagators provide the Q^2 -dependence.

It is important to note that the non-diagonal terms, $\Sigma_{n,n'}$ with $n \neq n'$, are essential in the GVMD model: The infinite series in Eq. (3) would have been divergent without the non-diagonal transitions. Also, the non-diagonal terms provide the correct scaling of the total $\gamma^* p$ cross section.

Using Eqs. (4) and (5), the DVCS amplitude in Eq. (3) can be written in the following form

$$\begin{aligned} \mathcal{A}(\gamma_{\text{tr}}^* + p \rightarrow \gamma + p) = & i \frac{2(1+\delta)e^2}{f_\rho^2} \sigma_{\rho p}(W^2)(1-i\eta) \sum_{n=0}^{\infty} \frac{F_n(t)}{(\frac{Q^2}{m_\rho^2} + 1 + 2n)(\frac{Q^2}{m_\rho^2} + 3 + 2n)} \\ & \times \left[1 + \frac{Q^2}{2m_\rho^2(1+\delta)(3+2n)} \left(1 + 4\delta \frac{1+n}{(1+2n)} \right) \right]. \end{aligned} \quad (7)$$

Equation (7) involves four quantities, f_ρ , $\sigma_{\rho p}$, η and δ , which are known with a certain degree of uncertainty. One can reduce this uncertainty by expressing the DVCS amplitude in terms

of the total γp cross section,

$$\begin{aligned}\sigma_{\text{tot}}^{\gamma p}(W^2) &= \Im m \mathcal{A}(\gamma + p \rightarrow \gamma + p)|_{t=0} = \frac{2(1+\delta)e^2}{f_\rho^2} \sigma_{\rho p}(W^2) \sum_{n=0}^{\infty} \frac{1}{(1+2n)(3+2n)} \\ &= \frac{(1+\delta)e^2}{f_\rho^2} \sigma_{\rho p}(W^2).\end{aligned}\quad (8)$$

Therefore, the final expression for the DVCS amplitude reads

$$\begin{aligned}\mathcal{A}(\gamma_{\text{tr}}^* + p \rightarrow \gamma + p) &= i2 \sigma_{\text{tot}}^{\gamma p}(W^2)(1 - i\eta) \sum_{n=0}^{\infty} \frac{F_n(t)}{(\frac{Q^2}{m_\rho^2} + 1 + 2n)(\frac{Q^2}{m_\rho^2} + 3 + 2n)} \\ &\times \left[1 + \frac{Q^2}{2m_\rho^2(1+\delta)(3+2n)} \left(1 + 4\delta \frac{1+n}{(1+2n)} \right) \right].\end{aligned}\quad (9)$$

One should also note that another advantage of expressing the DVCS amplitude in terms of $\sigma_{\text{tot}}^{\gamma p}$ is that Eq. (9) effectively takes into account the contributions of the ω and ϕ vector mesons, which enter through the phenomenological parameterization of $\sigma_{\text{tot}}^{\gamma p}$.

In our analysis, we use the ZEUS parameterization of $\sigma_{\text{tot}}^{\gamma p}(W^2)$ [47]

$$\sigma_{\text{tot}}^{\gamma p}(W^2) = 57 W^{0.2} + 121 W^{-0.716}, \quad (10)$$

where the cross section is in μb and W is in GeV.

The ratio of the real to imaginary parts of the $V + p \rightarrow V + p$ scattering amplitude, η , is found using the Gribov-Migdal relation [48],

$$\eta \approx \frac{\pi}{2} \frac{p}{2} \approx 0.16, \quad (11)$$

where $p = 0.2$ was used, which corresponds to the power of the W -dependence of $\sigma_{\text{tot}}^{\gamma p}(W^2)$ at large W in Eq. (10).

The remaining parameter in Eq. (9) is δ , for which we use $\delta = 0.2$ [26, 27, 28, 46]. However, the exact numerical value of δ affects weakly our numerical predictions.

One of simplest DVCS observables is the skewing factor R , which is defined as the ratio of the DVCS to the DIS amplitudes and which was recently extracted from the HERA DVCS and DIS data [49],

$$R(t) \equiv \frac{\Im m \mathcal{A}(\gamma_{\text{tr}}^* + p \rightarrow \gamma + p)|_t}{\Im m \mathcal{A}(\gamma_{\text{tr}}^* + p \rightarrow \gamma_{\text{tr}}^* + p)|_{t=0}}. \quad (12)$$

Note that we generalized the ratio R originally defined at $t = t_{\text{min}}$ [49] to any value of t . At high energies, the minimal momentum transfer $|t_{\text{min}}| \approx x_B^2 m_N^2 \approx 0$, where x_B is the Bjorken variable; m_N is the nucleon mass.

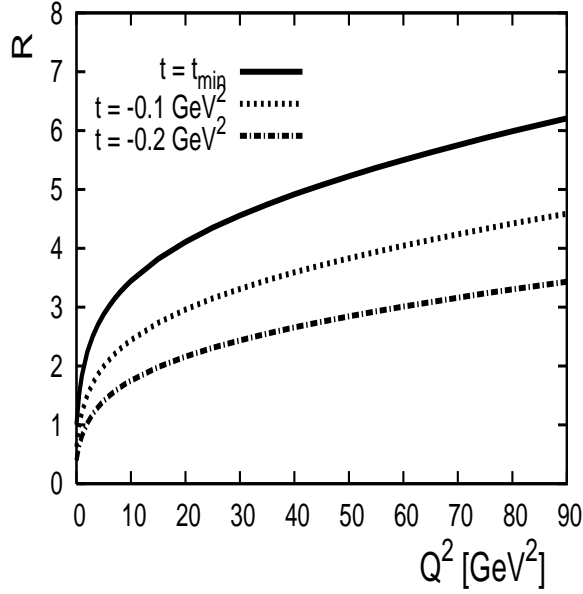


FIG. 2: The GVMD prediction for the ratio $R(t)$ of the DVCS and DIS amplitudes, see Eq. (12), as a function of Q^2 for three values of t .

The GVMD model makes an unambiguous prediction for the ratio R ,

$$R(t) = \sum_{n=0}^{\infty} \frac{F_n(t)}{(\frac{Q^2}{m_\rho^2} + 1 + 2n)(\frac{Q^2}{m_\rho^2} + 3 + 2n)} \left[1 + \delta + \frac{Q^2}{2m_\rho^2(3 + 2n)} \left(1 + 4\delta \frac{1 + n}{(1 + 2n)} \right) \right] \\ / \left(\sum_{n=0}^{\infty} \frac{1 + 2n}{(\frac{Q^2}{m_\rho^2} + 1 + 2n)^2 (\frac{Q^2}{m_\rho^2} + 3 + 2n)} + \frac{1}{2} \frac{\delta}{1 + \frac{Q^2}{m_\rho^2}} \right). \quad (13)$$

Figure 2 presents the GVMD predictions for the ratio R as a function of Q^2 for three values of t : $t = t_{\min} \approx 0$ (evaluated with $x_B = 0.001$), $t = -0.1 \text{ GeV}^2$ and $t = -0.2 \text{ GeV}^2$. Note that in the GVMD model, the ratio R does not depend on W or x_B at given Q^2 and t .

A comparison of the solid curve in Fig. 2 to the experimental results for the ratio R , see Fig. 4 of Ref. [49], reveals that the GVMD model provides a good description of the data for $Q^2 < 5 \text{ GeV}^2$. For higher values of Q^2 , the GVMD model overestimates the experimental R . Therefore, the GVMD model and similar models can be used to reliably determine DVCS observables and generalized parton distributions at Q^2 of the order of a few GeV^2 . This can be used as an input for QCD evolution to higher Q^2 scales. An example of such an approach, which uses the align-jet model to construct input GPDs and which excellently compares to

the HERA data on the DVCS cross section and on the ratio R , was worked out in [50].

B. DVCS cross section

The DVCS amplitude in Eq. (9) is normalized such that in the $Q^2 \rightarrow 0$ limit, the imaginary part of the $\gamma p \rightarrow \gamma p$ amplitude is equal to the total photoabsorption cross section, see Eq. (8). With such a normalization, the differential and integrated DVCS cross sections at the photon level read

$$\begin{aligned}\frac{d\sigma_{\text{DVCS}}}{dt}(W, Q^2, t) &= \frac{1}{16\pi} |\mathcal{A}(\gamma_{\text{tr}}^* + p \rightarrow \gamma + p)|^2, \\ \sigma_{\text{DVCS}}(W, Q^2) &= \frac{1}{16\pi} \int_{-1}^{t_{\text{min}}} dt |\mathcal{A}(\gamma_{\text{tr}}^* + p \rightarrow \gamma + p)|^2.\end{aligned}\quad (14)$$

where $t_{\text{min}} \approx -x_B^2 m_N^2$ ($t_{\text{min}} \approx 0$ in the HERA kinematics).

In order to compare the GVMD model predictions to the data on the DVCS cross section at the photon level [30, 31], one needs to make sure that one compares the same quantities. Using the classic result of L. N. Hand [51], one can readily see that the HERA DVCS cross section at the photon level is indeed a properly defined and normalized cross section of the $\gamma^* p \rightarrow \gamma p$ reaction.

As a byproduct of the above mentioned exercise, one establishes the connection between the GVMD and GPD descriptions of the DVCS cross section:

$$\begin{aligned}|\mathcal{A}(\gamma_{\text{tr}}^* + p \rightarrow \gamma + p)|^2 &= \frac{e^4 x_B^2}{Q^4 \sqrt{1 + \epsilon^2}} \left((1 - \xi^2)(|\mathcal{H}|^2 + |\tilde{\mathcal{H}}|^2) - \xi^2(\mathcal{H}^* \mathcal{E} + \mathcal{H} \mathcal{E}^* \right. \\ &\quad \left. + \tilde{\mathcal{H}}^* \tilde{\mathcal{E}} + \tilde{\mathcal{H}} \tilde{\mathcal{E}}^*) - |\mathcal{E}|^2 \left(\frac{t}{4m_N^2} + \xi^2 \right) - \xi^2 \frac{t}{4m_N^2} |\tilde{\mathcal{E}}|^2 \right),\end{aligned}\quad (15)$$

where x_B is the Bjorken variable; $\xi = x_B/(2 - x_B)$; $\epsilon^2 = 4x_B^2 m_N^2/Q^2$. The quantities \mathcal{H} , \mathcal{E} , $\tilde{\mathcal{H}}$ and $\tilde{\mathcal{E}}$ are the so-called Compton form factors of the corresponding proton GPDs [12]. It is important to have the connection between the GVMD-based and the GPD-based descriptions of the DVCS cross section since the both approaches have an overlapping region of applicability, namely, $1 < Q^2 < 5 \text{ GeV}^2$.

The simple expression for the DVCS amplitude in the GVMD model (9) allows one to examine the relative contribution of $1/Q^2$ -corrections, which correspond to higher-twist corrections in perturbative QCD. To this end, let us expand the DVCS amplitude in Eq. (9) in terms of $1/Q^2$ and let us call the leading contribution, which behaves as $1/Q^2$, $\mathcal{A}^{\text{LO}}(\gamma_{\text{tr}}^* + p \rightarrow \gamma + p)$. The corresponding t -integrated cross section is denoted as $\sigma_{\text{DVCS}}^{\text{LO}}$.

TABLE I: The $1/Q^2$ -corrections to the DVCS amplitude and to the t -integrated DVCS cross section as functions of Q^2 , see Eq. (16).

Q^2 [GeV ²]	$R_{\text{ampl}}^{\text{HT}}(Q^2)$	$R_{\sigma}^{\text{HT}}(Q^2)$
2	0.20	0.56
4	0.11	0.32
8	0.058	0.17

We quantify the contribution of $1/Q^2$ -corrections to the DVCS amplitude and to the DVCS cross section by introducing the ratios $R_{\text{ampl}}^{\text{HT}}$ and R_{σ}^{HT} ,

$$\begin{aligned}
R_{\text{ampl}}^{\text{HT}}(Q^2) &= 1 - \frac{\mathcal{A}^{\text{LO}}(\gamma_{\text{tr}}^* + p \rightarrow \gamma + p)|_{t=t_{\text{min}}}}{\mathcal{A}(\gamma_{\text{tr}}^* + p \rightarrow \gamma + p)|_{t=t_{\text{min}}}}, \\
R_{\sigma}^{\text{HT}}(Q^2) &= 1 - \frac{\sigma_{\text{DVCS}}^{\text{LO}}}{\sigma_{\text{DVCS}}}.
\end{aligned} \tag{16}$$

The ratios $R_{\text{ampl}}^{\text{HT}}$ and R_{σ}^{HT} as functions of Q^2 are summarized in Table I. Note that these ratios do not depend on W in the chosen model.

As one can see from Table I, the $1/Q^2$ -corrections are large. Moreover, $R_{\sigma}^{\text{HT}}(Q^2) > 2R_{\text{ampl}}^{\text{HT}}(Q^2)$ due to the enhancement of the heavy vector meson contributions to σ_{DVCS} because of the decreasing slope of the t -dependence of the DVCS amplitude with increasing n , see Eq. (6).

C. Comparison to the HERA DVCS data

Using Eqs. (9) and (14), we make predictions for the DVCS cross section and compare our findings to the HERA data [30, 31].

Figure 3 presents the W -dependence of the DVCS cross section at $Q^2 = 4 \text{ GeV}^2$ and $Q^2 = 8 \text{ GeV}^2$. The solid curves correspond to the GVMD calculations; the experimental points are those from the H1 [31] and ZEUS [30] measurements. The error bars correspond to the statistical and systematic errors added in quadrature. The ZEUS data taken at $Q^2 = 9.6 \text{ GeV}^2$ have been interpolated to $Q^2 = 8.0 \text{ GeV}^2$ using the fit to the Q^2 -dependence of σ_{DVCS} , $\sigma_{\text{DVCS}} \sim 1/(Q^2)^n$ with $n = 1.54$ [30].

We shall discuss the left and right panels of Fig. 3 separately. As seen from the left panel of Fig. 3, the GVMD model reproduces both the absolute value and the W -dependence of

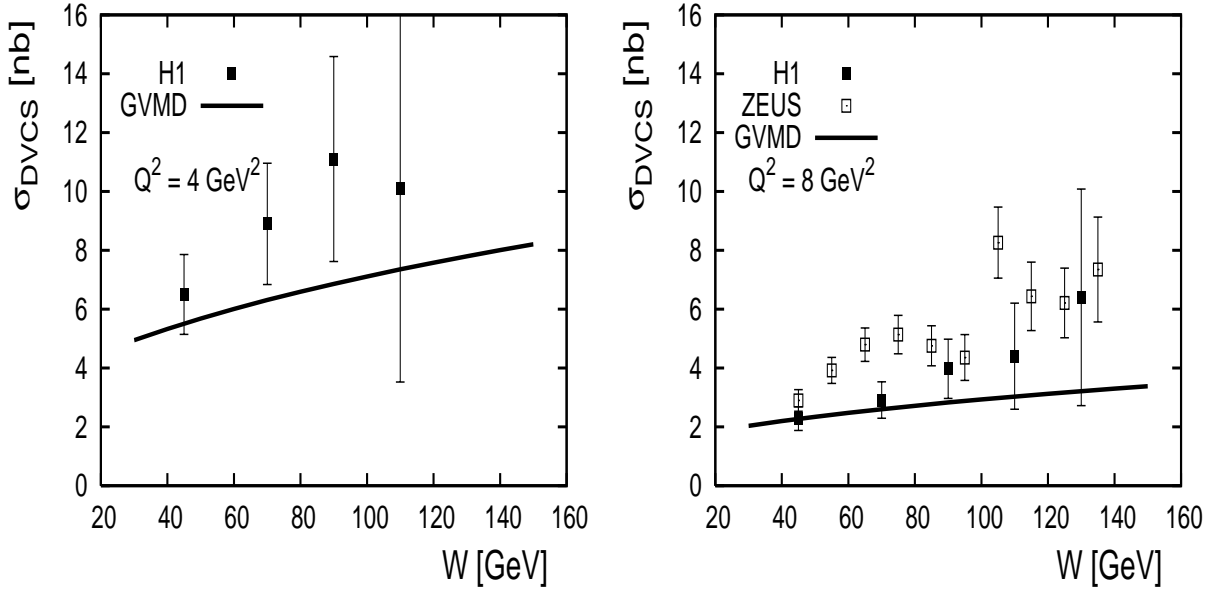


FIG. 3: The DVCS cross section as a function of W . The GVMD model results (solid curves) are compared to the H1 [31] and ZEUS [30] data. The error bars correspond to the statistical and systematic errors added in quadrature.

σ_{DVCS} sufficiently well. The latter fact signifies that, at $Q^2 = 4 \text{ GeV}^2$, the DVCS cross section is still dominated by soft physics. At $Q^2 = 4 \text{ GeV}^2$, the W -behavior of σ_{DVCS} is consistent with that predicted by the GVMD model, $\sigma_{\text{DVCS}} \sim W^{0.4}$.

Turning to the right panel of Fig. 3, we observe that while the GVMD model compares fairly with the H1 data, the model underestimates the slope of the W -dependence of σ_{DVCS} for the ZEUS data set, which has smaller error bars. In particular, the predicted $\sigma_{\text{DVCS}} \sim W^{0.4}$ behavior is much slower than that given by the fit to the ZEUS data points, $\sigma_{\text{DVCS}} \sim W^\delta$ with $\delta = 0.75 \pm 0.15$ [30]. This indicates the onset of the hard regime in the total DVCS cross section at $Q^2 = 8 \text{ GeV}^2$, where the GVMD model becomes inadequate.

Figure 4 presents the Q^2 -dependence of the DVCS cross section at $W = 82 \text{ GeV}$. The solid curve corresponds to the GVMD model; the experimental points come from the H1 [31] and ZEUS [30] experiments. The error bars correspond to the statistical and systematic errors added in quadrature. The ZEUS data taken at $W = 89 \text{ GeV}$ have been extrapolated to $W = 82 \text{ GeV}$ using the fitted W -dependence of σ_{DVCS} , $\sigma_{\text{DVCS}} \sim W^{0.75}$ [30].

One sees from Fig. 4 that the GVMD model reproduces the Q^2 -dependence of σ_{DVCS} over a very wide range of Q^2 , $3 \leq Q^2 \leq 85 \text{ GeV}^2$. This is quite a remarkable result that

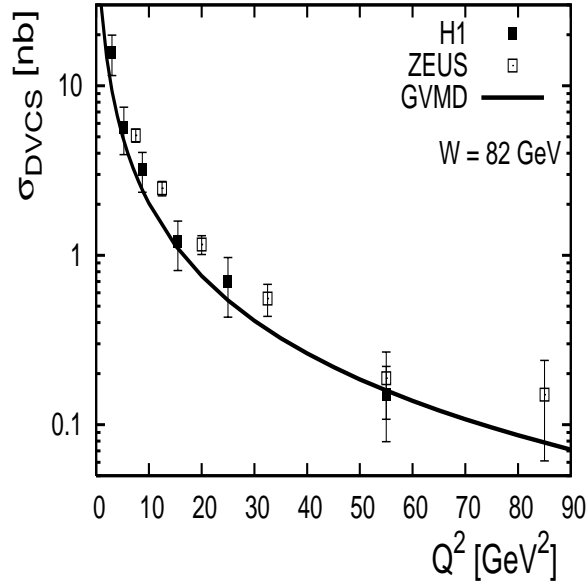


FIG. 4: The DVCS cross section as a function of Q^2 . The GVMD model result (solid curve) is compared to the H1 [31] and ZEUS [30] data. The error bars correspond to the statistical and systematic errors added in quadrature.

the model, which was initially developed for photoproduction and was later extended to electroproduction with Q^2 of the order of a few GeV^2 , provides a quantitative description for such large values of Q^2 . In other words, at fixed W , the GVMD model correctly reproduces the Q^2 -scaling of σ_{DVCS} .

Figure 5 presents the comparison of the t -dependence of the GVMD model calculations (solid curves) to the H1 data on the differential DVCS cross section $d\sigma_{\text{DVCS}}/dt$ [31]. The error bars are the statistical and systematic errors added in quadrature.

As one sees from Fig. 5, the GVMD model describes $d\sigma_{\text{DVCS}}/dt$ well. This result is not quite trivial. In order to achieve this within the framework of the GVMD model, one has to assume that either all vector meson V_n -nucleon cross sections have the same Q^2 -dependent slope of the t -dependence or that the slope decreases with increasing n , see Eq. (6). While the value of the slope $B_1 = 11 \text{ GeV}^{-2}$ is fixed by photoproduction of ρ mesons, the value of the slope B_2 is model-dependent. The values $B_2 = 4 \div 5 \text{ GeV}^{-2}$ provide a good agreement with the H1 data (see Fig. 5), which were fitted to the exponential form, $d\sigma_{\text{DVCS}}/dt \sim e^{-B|t|}$ with $B = (6.66 \pm 0.54 \pm 0.43) \text{ GeV}^{-2}$ at $Q^2 = 4 \text{ GeV}^2$ and $B = (5.82 \pm 0.59 \pm 0.60) \text{ GeV}^{-2}$ at $Q^2 = 8 \text{ GeV}^2$ [31].

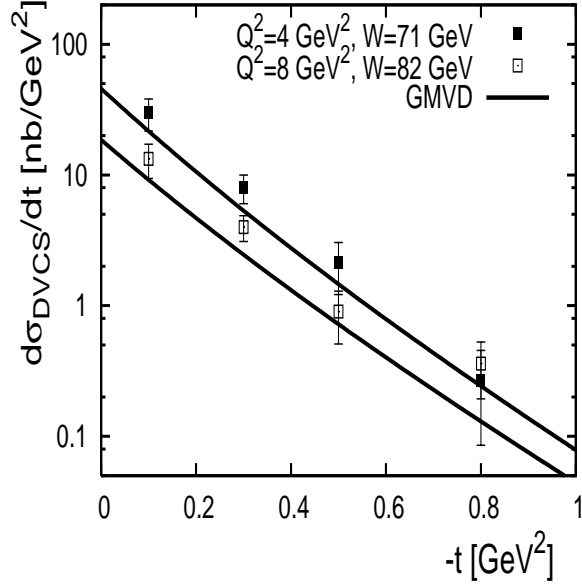


FIG. 5: The differential DVCS cross section $d\sigma_{\text{DVCS}}/dt$ as a function of t . The GVMD model calculation (solid curves) is compared to the H1 data [31]. The error bars are the statistical and systematic errors added in quadrature.

D. DVCS cross section in Jefferson Lab kinematics

The $\vec{e}p \rightarrow ep\gamma$ cross section in the DVCS regime was recently measured by the Hall A collaboration at Jefferson Laboratory (JLab) [24]. The cross section involves the contributions of the Bethe-Heitler (BH) amplitude squared, the DVCS amplitude squared and the interference of the BH and DVCS amplitudes. Based on the kinematics of the experiment, in the analysis of the data, the contribution of the DVCS amplitude squared was neglected compared to the other two contributions [12], which allowed for the extraction of the so-called Compton form factors of the proton.

In this subsection, we check the validity of the assumption that the contribution of the DVCS amplitude squared is negligibly small by explicitly calculating the DVCS cross section within the GVMD model in the Jefferson Lab kinematics. The DVCS cross section at the lepton level reads, see e.g. [12],

$$\frac{d^4\sigma}{dQ^2 dx_B dt d\phi} = \frac{\alpha_{\text{e.m.}}(1-y+y^2/2)}{\pi Q^2 x_B} \frac{1}{2\pi} \frac{d\sigma_{\text{DVCS}}(W, Q^2, t)}{dt}, \quad (17)$$

where $\alpha_{\text{e.m.}}$ is the fine-structure constant; ϕ is the angle between the lepton and production

planes; $d\sigma_{\text{DVCS}}(W, Q^2, t)/dt$ is the DVCS cross section at the proton level defined by Eq. (14). The extra factor $1/(2\pi)$ in the right-hand side of Eq. (17) takes into account the fact that the integration over the angle ϕ is included in the definition of $d\sigma_{\text{DVCS}}(W, Q^2, t)/dt$. The DVCS cross section does not depend on ϕ when one neglects the photon helicity changing transitions [11].

Using Eqs. (9) and (14), we evaluate the DVCS cross section at the lepton level $d^4\sigma/(dQ^2 dx_B dt d\phi)$ in the kinematics of the Hall A experiment, $E = 5.75$ GeV (the energy of the lepton beam), $Q^2 = 2.3$ GeV, $t = -0.28$ GeV and $x_B = 0.36$,

$$\frac{d^4\sigma}{dQ^2 dx_B dt d\phi} = 0.0022 \text{ nb/GeV}^4. \quad (18)$$

This value is an order of magnitude smaller than the sum of the BH and interference contributions to the $ep \rightarrow ep\gamma$ cross section, which confirms the assumption that, in the JLab kinematics, the contribution of the DVCS amplitude squared to the $ep \rightarrow ep\gamma$ cross section can be safely neglected.

III. DVCS ON NUCLEI

In this section, we derive the expression for the DVCS amplitude on a nucleus using the GVMD model for the photon-nucleon interactions and the generalized Glauber formalism [37] in order to account for the multiple rescattering of the vector mesons inside the nucleus. Using the obtained amplitude, we make predictions for the nuclear DVCS cross section at the photon level in the collider kinematics.

At high energies, in the GVMD model, photons (real and virtual) interact with hadrons by fluctuating into an infinite sum of vector mesons. When the involved hadron is a nucleus, each vector meson undergoes multiple interactions with the nucleons of the nucleus, which leads to the attenuation (decrease) of the vector meson-nucleus cross section compared to the sum of free vector meson-nucleon cross section. As a consequence, the resulting photon-nucleus cross section is smaller than the sum of the corresponding photon-nucleon cross sections. This phenomenon is called nuclear shadowing. It has been observed in various reactions with nuclei induced by real and virtual photons, see [37, 52] for review.

In the GVMD model, the nuclear DVCS amplitude can be organized as a multiple scattering series (Glauber series), where each term corresponds to the number of interactions of

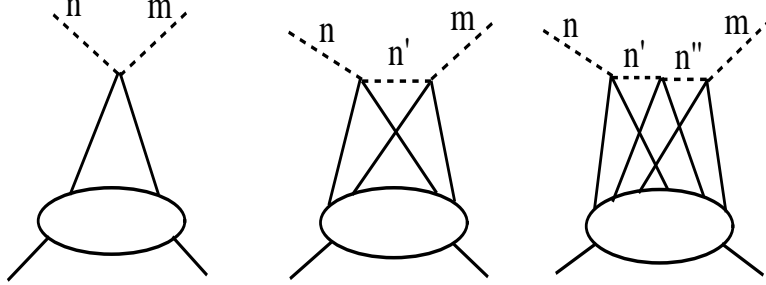


FIG. 6: A schematic representation of the multiple scattering (Glauber) series for the nuclear DVCS amplitude in the GVMD model. The dashed lines correspond to vector mesons; the solid lines correspond to nucleons; the ovals with legs correspond to the final and initial nucleus.

the vector mesons with the nucleons. This is schematically presented in Fig. 6, where the interactions with one, two and three nucleons are depicted. The dashed lines correspond to the vector mesons (note that the GVMD model allows for non-diagonal vector meson-nucleon transitions); the solid lines correspond to the nucleons involved in the interactions; the nuclear part is denoted by ovals with legs corresponding to the initial and final nucleus.

Using the standard technique [37], one can readily write down the expression for the nuclear DVCS amplitude $\mathcal{A}(\gamma^* + A \rightarrow \gamma + A)$,

$$\begin{aligned}
\mathcal{A}(\gamma^* + A \rightarrow \gamma + A) = & \sum_{n,m=0}^{\infty} \frac{e}{f_n} \frac{M_n^2}{M_n^2 + Q^2} \frac{e}{f_m} \left[AF_A(t) \Sigma_{n,m}(W, t) \right. \\
& - \frac{A(A-1)}{2i} \int_{-\infty}^{\infty} dz_1 \int_{z_1}^{\infty} dz_2 \int d^2\vec{b} e^{i\vec{q}_t \cdot \vec{b}} \rho(b, z_1) \rho(b, z_2) e^{iz_1(k_{\gamma^*} - k_{V_n})} \\
& \times \tilde{\Sigma}_{n,n'}(W, z_1) \left(\delta_{n',n''} - \frac{A-2}{2i} \tilde{\Sigma}_{n',n''}(W, z') \Theta(z_1 \leq z' \leq z_2) \rho(b, z') \right. \\
& \left. \left. + \dots \right) \tilde{\Sigma}_{n'',m}(W, z_2) e^{iz_2(k_{V_m} - k_{\gamma})} \right], \tag{19}
\end{aligned}$$

where A is the number of nucleons in the nucleus (we do not distinguish protons and neutrons); $F_A(t)$ is the nuclear form factor ($F_A(0) = 1$); $\rho(r)$ is the density of nucleons in the

nucleus [53]; \vec{b} is the two-dimensional vector (impact parameter) in the plane perpendicular to the direction of the incoming photon, whose momentum is assumed to be along the z -direction; z_i are longitudinal positions of the nucleons of the nucleus involved in the interaction; \vec{q}_t is the transverse component of the momentum transfer. Since we neglected the t -dependence of the elementary vector meson-nucleon scattering amplitudes compared to the steep t -dependence of the nuclear form factor, all scatterings of the vector mesons in Eq. (19) occur at the same impact parameter \vec{b} .

In Eq. (19),

$$\tilde{\Sigma}_{n,m}(W, z) = e^{iz(k_{V_n} - k_{V_m})} \Sigma_{n,m}(W, t = 0), \quad (20)$$

where $\Sigma_{n,m}$ is defined by Eq. (5). In Eqs. (19) and (20), the exponential factors (except for the $\exp(i\vec{q}_t \cdot \vec{b})$ factor) arise due to the non-zero longitudinal momentum transfer associated with non-diagonal in mass transitions. At high energies,

$$\begin{aligned} k_{\gamma^*} - k_{V_n} &= \sqrt{\nu^2 + Q^2} - \sqrt{\nu^2 - M_n^2} = \frac{Q^2 + M_n^2}{2\nu} = x_B m_N \left(1 + \frac{M_n^2}{Q^2} \right), \\ k_{V_m} - k_{\gamma} &= \sqrt{\nu'^2 - M_m^2} - \nu' = -\frac{M_m^2}{2\nu'} \approx -\frac{M_m^2}{2\nu} = -x_B m_N \frac{M_m^2}{Q^2}, \\ k_{V_n} - k_{V_m} &= \frac{M_m^2 - M_n^2}{2\nu}, \end{aligned} \quad (21)$$

where ν is the energy of the incoming virtual photon in the laboratory reference frame; ν' is the energy of the final real photon. We also used that $\nu' = \nu + t/(2m_N) \approx \nu$ for the small momentum transfer t .

In Eq. (19), the first term corresponds to the left graph in Fig. 6, which describes the interaction with one nucleon of the nucleus (the Born term). The second term in Eq. (19) corresponds to the middle graph in Fig. 6, which describes the interaction of hadronic fluctuations of the involved photons with two nucleons of the nucleus. Those nucleons are located at the points $\vec{r}_1 = (\vec{b}, z_1)$ and $\vec{r}_2 = (\vec{b}, z_2)$. This graph leads to the attenuation (nuclear shadowing) of the Born term. The third term corresponds to the interaction with three nucleons of the nucleus. The dots in Eq. (19) denote higher rescattering terms not shown in Fig. 6.

Equation (19) is rather general and, because of the non-diagonal $V_n \rightarrow V_{n'}$ transitions, the direct calculation of the nuclear DVCS amplitude for heavy nuclei using Eq. (19) is impossible. Therefore, for our numerical predictions, we make an approximation and ignore

the non-diagonal transitions for the interactions with three and more nucleons (this does affect the convergence of the series),

$$\begin{aligned}
& \delta_{n',n''} - \frac{A-2}{2i} \tilde{\Sigma}_{n',n''}(W, z') \Theta(z_1 \leq z' \leq z_2) \rho(b, z') + \dots \\
& \rightarrow \delta_{n',n''} \left(1 - \frac{A-2}{2i} \Sigma_{n',n'}(W, t=0) \Theta(z_1 \leq z' \leq z_2) \rho(b, z') + \dots \right) \\
& = \delta_{n',n''} e^{-\frac{A}{2} \sigma_{pp}(W^2)(1-i\eta) \int_{z_1}^{z_2} dz' \rho(b, z')}, \tag{22}
\end{aligned}$$

where in the last line we used the large- A approximation. Therefore, Eq. (19) now reads

$$\begin{aligned}
\mathcal{A}(\gamma^* + A \rightarrow \gamma + A) &= \sum_{n,m=0}^{\infty} \frac{e}{f_n} \frac{M_n^2}{M_n^2 + Q^2} \frac{e}{f_m} \left[AF_A(t) \Sigma_{n,m}(W, t) \right. \\
&\quad - \frac{A(A-1)}{2i} \int_{-\infty}^{\infty} dz_1 \int_{z_1}^{\infty} dz_2 \int d^2 \vec{b} e^{i \vec{q} \cdot \vec{b}} \rho(b, z_1) \rho(b, z_2) e^{iz_1(k_{\gamma^*} - k_{V_n})} \\
&\quad \times \tilde{\Sigma}_{n,n'}(W, z_1) e^{-\frac{A}{2} \sigma_{pp}(W^2)(1-i\eta) \int_{z_1}^{z_2} dz' \rho(b, z')} \tilde{\Sigma}_{n',m}(W, z_2) e^{iz_2(k_{V_m} - k_{\gamma})} \left. \right]. \tag{23}
\end{aligned}$$

For comparison of nuclear shadowing in DVCS and DIS, we also give the expression for the forward nuclear DIS amplitude, which can be readily obtained from Eq. (23),

$$\begin{aligned}
\mathcal{A}(\gamma^* + A \rightarrow \gamma^* + A)|_{t=0} &= \sum_{n,m=0}^{\infty} \frac{e}{f_n} \frac{M_n^2}{M_n^2 + Q^2} \frac{e}{f_m} \frac{M_m^2}{M_m^2 + Q^2} \left[A \Sigma_{n,m}(W, t=0) \right. \\
&\quad - \frac{A(A-1)}{2i} \int_{-\infty}^{\infty} dz_1 \int_{z_1}^{\infty} dz_2 \int d^2 \vec{b} \rho(b, z_1) \rho(b, z_2) e^{iz_1(k_{\gamma^*} - k_{V_n})} \\
&\quad \times \tilde{\Sigma}_{n,n'}(W, z_1) e^{-\frac{A}{2} \sigma_{pp}(W^2)(1-i\eta) \int_{z_1}^{z_2} dz' \rho(b, z')} \tilde{\Sigma}_{n',m}(W, z_2) e^{iz_2(k_{V_m} - k_{\gamma^*})} \left. \right]. \tag{24}
\end{aligned}$$

We quantify predictions of the GVMD model for the nuclear DVCS and DIS amplitudes by considering the ratios $R_{\text{ampl}}^{\text{Im}}$, $R_{\text{ampl}}^{\text{Re}}$ and $R_{\text{ampl}}^{\text{DIS}}$,

$$\begin{aligned}
R_{\text{ampl}}^{\text{Im}} &= \frac{\Im m \mathcal{A}(\gamma^* + A \rightarrow \gamma + A)}{\Im m \mathcal{A}^{\text{Born}}(\gamma^* + A \rightarrow \gamma + A)}, \\
R_{\text{ampl}}^{\text{Re}} &= \frac{\Re e \mathcal{A}(\gamma^* + A \rightarrow \gamma + A)}{\Re e \mathcal{A}^{\text{Born}}(\gamma^* + A \rightarrow \gamma + A)}, \\
R_{\text{ampl}}^{\text{DIS}} &= \frac{\Im m \mathcal{A}(\gamma^* + A \rightarrow \gamma^* + A)|_{t=0}}{\Im m \mathcal{A}^{\text{Born}}(\gamma^* + A \rightarrow \gamma^* + A)|_{t=0}}, \tag{25}
\end{aligned}$$

where $\mathcal{A}(\gamma^* + A \rightarrow \gamma + A)$ is the nuclear DVCS amplitude of Eq. (23); $\mathcal{A}^{\text{Born}}(\gamma^* + A \rightarrow \gamma + A)$ is the first term (Born contribution) of Eq. (23); $\mathcal{A}^{\text{Born}}(\gamma^* + A \rightarrow \gamma^* + A)|_{t=0}$ is the first term of Eq. (26). Note that $R_{\text{ampl}}^{\text{DIS}}$ is nothing but the ratio of the nuclear to the nucleon inclusive structure functions, $R_{\text{ampl}}^{\text{DIS}} = F_{2A}(x, Q^2)/[AF_{2N}(x, Q^2)]$.

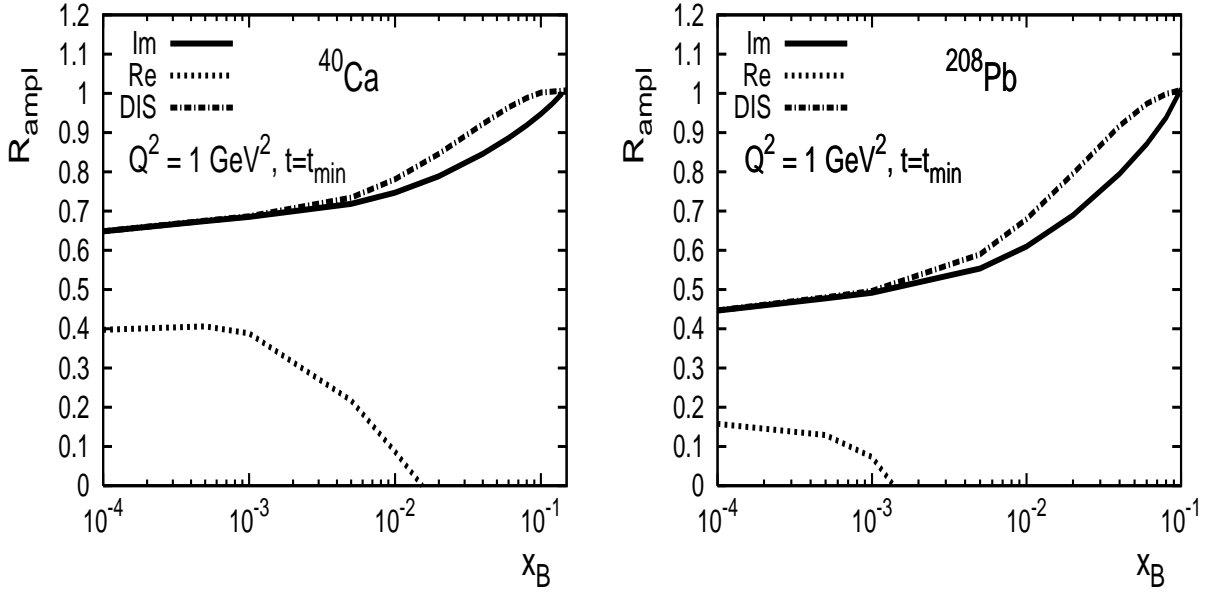


FIG. 7: The ratios $R_{\text{ampl}}^{\text{Im}}$ (solid), $R_{\text{ampl}}^{\text{Re}}$ (dotted) and $R_{\text{ampl}}^{\text{DIS}}$ (dot-dashed) of Eq. (25) at $Q^2 = 1 \text{ GeV}^2$ and $t = t_{\text{min}}$ as functions of Bjorken x_B . The left panel is for ^{40}Ca ; the right panel is for ^{208}Pb .

Figure 7 presents the ratios $R_{\text{ampl}}^{\text{Im}}$ (solid curves), $R_{\text{ampl}}^{\text{Re}}$ (dotted curves) and $R_{\text{ampl}}^{\text{DIS}}$ (dot-dashed curves) at $Q^2 = 1 \text{ GeV}^2$ and $t = t_{\text{min}} \approx -x_B^2 m_N^2$ as functions of x_B . The left panel corresponds to the nucleus of ^{40}Ca ; the right panel corresponds to ^{208}Pb .

Let us now discuss the results presented in Fig. 7 in detail. The solid and dot-dashed curves coincide for $x_B < 0.01$ and deviate only slightly for $0.01 < x_B < 0.1$, which means that the amount of nuclear shadowing is the same in the imaginary parts of the DVCS and DIS amplitudes. This observation agrees with the results obtained within the framework of a different approach to nuclear GPDs at small- x_B , when the latter are modeled using the align-jet model for the nucleon GPDs and a parameterization of usual nuclear PDFs [54]. Moreover, the amount of nuclear shadowing predicted by our calculations in the GVMD model matches very well the leading-twist predictions for $F_{2A}(x, Q^2)/[AF_{2N}(x, Q^2)]$ made at somewhat higher Q^2 [35]. This is a consequence of the fact the GVMD model predicts a significant amount of inclusive diffraction in γ^*p scattering at all Q^2 , which controls the size of nuclear shadowing in the leading-twist theory of nuclear shadowing [35].

As the value of x_B is increased (at fixed Q^2), the shadowing correction decreases due to the decrease of $\sigma_{pp}(W)$ and due to the increasingly destructive role of the $e^{iz_1(k_{\gamma^*} - k_{V_n})}$ and

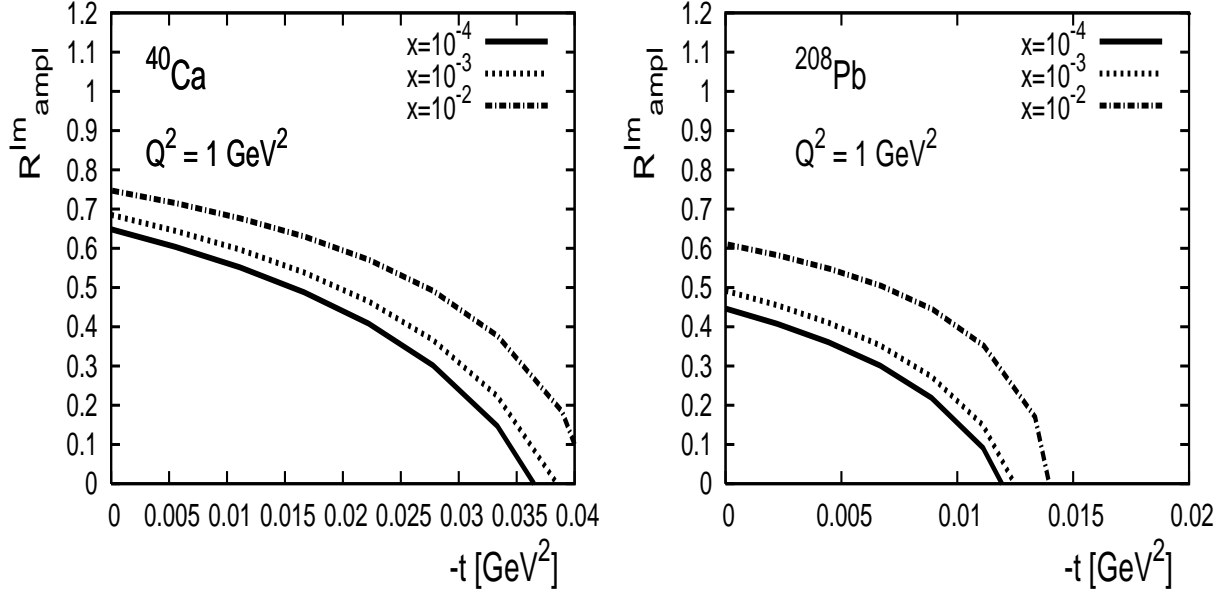


FIG. 8: The ratio $R_{\text{ampl}}^{\text{Im}}$ at $Q^2 = 1 \text{ GeV}^2$ as a function of t . The left panel is for ^{40}Ca ; the right panel is for ^{208}Pb .

$e^{iz_2(k_{V_m}-k_\gamma)}$ factors in Eq. (23).

For the ratio $R_{\text{ampl}}^{\text{Re}}$ of the real parts (dotted curves), at small- x_B , the shadowing correction is approximately two times as large as for the ratio of the imaginary parts because of the fact that $(1 - \eta)^2 = 1 - \eta^2 - 2i\eta$, see Eqs. (5) and (23). As x_B increases, the real part of the shadowing correction receives a large contribution from the $e^{iz_1(k_{\gamma^*}-k_{V_n})}$ and $e^{iz_2(k_{V_m}-k_\gamma)}$ factors, and, as a result, it steadily grows and becomes larger than the Born contribution. This behavior of $R_{\text{ampl}}^{\text{Re}}$ is similar to that observed in [54]. Note, however, that since the effect of t_{min} (the factor $F_A(t_{\text{min}})$ in the Born term) was not included in the analysis of [54], the agreement could be coincidental.

We also examined nuclear shadowing in DVCS with nuclear targets as a function of the momentum transfer t . Figure 8 presents $R_{\text{ampl}}^{\text{Im}}$ at $Q^2 = 1 \text{ GeV}^2$ as a function of t . Figure 8 demonstrates that the shadowing correction to the DVCS amplitude has the t -dependence which is slower than that of the Born term. As one increases $|t|$, the negative nuclear shadowing correction decreases slower than the Born term, which leads to a decrease of $R_{\text{ampl}}^{\text{Im}}$. The ratio $R_{\text{ampl}}^{\text{Re}}$ follows the similar trend.

Equation (23) presents the $\gamma^*A \rightarrow \gamma A$ scattering amplitude as a function of W , Q^2 and t . It also allows for the representation of the scattering amplitude as a function of W , Q^2

and \vec{b} , where \vec{b} is the impact parameter conjugate to \vec{q}_t ,

$$\begin{aligned} \mathcal{A}(\gamma^* + A \rightarrow \gamma + A) = & \sum_{n,m=0}^{\infty} \frac{e}{f_n} \frac{M_n^2}{M_n^2 + Q^2} \frac{e}{f_m} \left[A \int_{-\infty}^{\infty} dz e^{ix_B m_N z} \rho(b, z) \Sigma_{n,m}(W, 0) \right. \\ & - \frac{A(A-1)}{2i} \int_{-\infty}^{\infty} dz_1 \int_{z_1}^{\infty} dz_2 \rho(b, z_1) \rho(b, z_2) e^{iz_1(k_{\gamma^*} - k_{\gamma_n})} \\ & \times \tilde{\Sigma}_{n,n'}(W, z_1) e^{-\frac{A}{2}\sigma_{pp}(W^2)(1-in)} \int_{z_1}^{z_2} dz' \rho(b, z') \tilde{\Sigma}_{n',m}(W, z_2) e^{iz_2(kv_m - k_{\gamma})} \left. \right]. \end{aligned} \quad (26)$$

In the first term in Eq. (26), we took into account the non-zero longitudinal momentum transfer, $k_{\gamma^*} - k_{\gamma} = x_B m_N$, see Eq. (21), and also neglected the t -dependence of $\Sigma_{n,m}(t)$ compared to $F_A(t)$.

Using Eq. (26), the nuclear DVCS cross section can be expressed in the following compact form

$$\sigma_{\text{DVCS}}(W, Q^2) = \frac{1}{4} \int d^2\vec{b} |\mathcal{A}(\gamma^* + A \rightarrow \gamma + A)|^2. \quad (27)$$

In order to quantify predictions of the GVMD model for nuclear DVCS cross sections, we introduce the ratio R_{cs} ,

$$R_{\text{cs}} = \frac{\sigma_{\text{DVCS}}(W, Q^2)}{\sigma_{\text{DVCS}}^{\text{Born}}(W, Q^2)}, \quad (28)$$

where the numerator is calculated using Eq. (27) and the complete expression for the nuclear DVCS amplitude (26); the denominator is calculated using only the first term (Born contribution) in Eq. (26).

Predictions of the GVMD model for the ratio R_{cs} at $Q^2 = 1 \text{ GeV}^2$ as a function of x_B are presented in Fig. 9. The solid curve corresponds to ^{40}Ca ; the dotted curve corresponds to ^{208}Pb .

As one can see from Fig. 9, the predicted amount of nuclear shadowing at small- x_B is very large. Since the t -dependence of the nuclear DVCS amplitude is very steep, the dominant contribution to the t -integrated cross sections entering R_{cs} comes from the $t \approx t_{\text{min}}$ region. Therefore, the amount of nuclear shadowing for R_{cs} is equal roughly twice the amount of nuclear shadowing for $R_{\text{ampl}}^{\text{Im}}$, see Fig. 7.

Finally, we would also like to point out that for nuclear DVCS, the ratio of the imaginary parts of the DVCS and DIS amplitudes, see Eq. (12) and Fig. 2, is quite similar to the free nucleon case. This is a mere consequence of the fact that the structure of the Q^2 -dependence of the ratio is essentially the same in the DVCS on the nucleon and on nuclei.

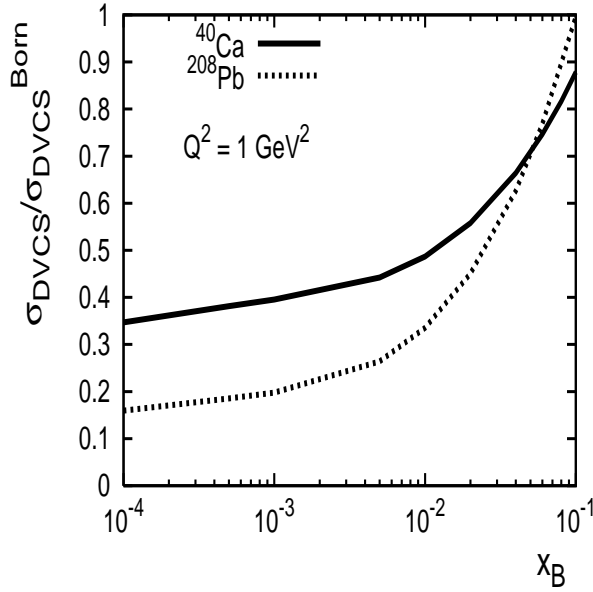


FIG. 9: The ratio $R_{\text{cs}} = \sigma_{\text{DVCS}}/\sigma_{\text{DVCS}}^{\text{Born}}$ of Eq. (28) as a function of Bjorken x_B at $Q^2 = 1 \text{ GeV}^2$. The solid curve corresponds to ^{40}Ca ; the dotted curve is for ^{208}Pb .

IV. CONCLUSIONS AND DISCUSSION

We considered Deeply Virtual Compton Scattering (DVCS) on nucleons and nuclei in the framework of generalized vector meson dominance (GVMD) model. We extended the original GVMD model, which was applied to forward amplitudes of Deep Inelastic Scattering (DIS), to the non-forward $t \neq 0$ case. We introduced the W -dependence of the DVCS amplitude through the W -dependence of the elementary vector meson-nucleon amplitude, which was taken to be proportional to $W^{0.2}$ at high- W .

We compared our predictions to the HERA data on DVCS on the proton with the following results. The GVMD model describes well the dependence of the DVCS cross section on Q^2 , W (at $Q^2=4 \text{ GeV}^2$) and t . At $Q^2=8 \text{ GeV}^2$, the W -dependence of the cross section is somewhat underestimated, which can be interpreted as due to the onset of the hard regime beyond the soft dynamics of the GVMD model.

We estimated the relative contribution of $1/Q^2$ -corrections to the DVCS amplitude and the DVCS cross section. We found that these corrections are large: the contribution of the $1/Q^2$ -corrections to the DVCS amplitude at $t = t_{\text{min}}$ is 20% at $Q^2 = 2 \text{ GeV}^2$, 11% at $Q^2 = 4 \text{ GeV}^2$ and 6% at $Q^2 = 8 \text{ GeV}^2$; the contribution of the $1/Q^2$ -corrections to the t -integrated

DVCS cross section is 56% at $Q^2 = 2 \text{ GeV}^2$, 32% at $Q^2 = 4 \text{ GeV}^2$ and 17% at $Q^2 = 8 \text{ GeV}^2$.

We also made predictions for the DVCS amplitude and the DVCS cross section on nuclear targets, which are relevant for the physics program of the future Electron-Ion Collider. We predicted significant nuclear shadowing, which matches well predictions of the leading-twist nuclear shadowing in DIS on nuclei.

Our analysis allows us to argue that the GVMD model provides a reliable parameterization of the DVCS amplitude and the DVCS cross section with nucleons and nuclei in a wide range of kinematics. At fixed values of Q^2 , which should not be too large, $Q^2 \lesssim 5 \text{ GeV}^2$, the GVMD model is applicable starting from $W = 2 \text{ GeV}$ (JLab), towards $W \approx 80 \text{ GeV}$ (HERA) and beyond (real photons at the LHC). At fixed W , the GVMD model is applicable from the photoproduction limit up to the values of Q^2 , where perturbative QCD can already be used, $0 \leq Q^2 \lesssim 5 \text{ GeV}^2$. In addition, due to the correct $1/Q^2$ -scaling, predictions of the GVMD model can be extrapolated to much higher values of Q^2 such that the range of applicability of the GVMD model becomes very wide, $0 \leq Q^2 < 80 \text{ GeV}^2$. The model can be applied for a wide range of t : $0 < |t| < 1 \text{ GeV}^2$.

Acknowledgments

The authors would like to thank C. Weiss for suggesting the research topic of the present paper and for useful discussions. We also thank M. Strikman for reading the manuscript and useful comments.

The work has been partially supported by the Verbundforschung ("Hadronen und Kerne") of the BMBF and by the Transregio/SFB Bonn-Bochum-Giessen.

Notice: Authored by Jefferson Science Associates, LLC under U.S. DOE Contract No. DE-AC05-06OR23177. The U.S. Government retains a non-exclusive, paid-up, irrevocable, world-wide license to publish or reproduce this manuscript for U.S. Government purposes.

-
- [1] D. Mueller, D. Robaschik, B. Geyer, F. M. Dittes and J. Horejsi, Fortsch. Phys. **42**, 101 (1994) [arXiv:hep-ph/9812448].
 - [2] X. D. Ji, Phys. Rev. D **55**, 7114 (1997).
 - [3] X. D. Ji, J. Phys. G **24**, 1181 (1998) [arXiv:hep-ph/9807358].

- [4] A. V. Radyushkin, Phys. Lett. B **380**, 417 (1996) [arXiv:hep-ph/9604317].
- [5] A. V. Radyushkin, Phys. Rev. D **56**, 5524 (1997).
- [6] A. V. Radyushkin, arXiv:hep-ph/0101225.
- [7] J. C. Collins and A. Freund, Phys. Rev. D **59**, 074009 (1999).
- [8] J. C. Collins, L. Frankfurt and M. Strikman, Phys. Rev. D **56**, 2982 (1997).
- [9] S. J. Brodsky, L. Frankfurt, J. F. Gunion, A. H. Mueller and M. Strikman, Phys. Rev. D **50**, 3134 (1994).
- [10] K. Goeke, M. V. Polyakov and M. Vanderhaeghen, Prog. Part. Nucl. Phys. **47**, 401 (2001) [arXiv:hep-ph/0106012].
- [11] M. Diehl, T. Feldmann, R. Jakob and P. Kroll, Nucl. Phys. B **596**, 33 (2001) [Erratum-ibid. B **605**, 647 (2001)] [arXiv:hep-ph/0009255].
- [12] A. V. Belitsky, D. Mueller and A. Kirchner, Nucl. Phys. B **629**, 323 (2002) [arXiv:hep-ph/0112108].
- [13] M. Diehl, Phys. Rept. **388**, 41 (2003) [arXiv:hep-ph/0307382].
- [14] A. V. Belitsky and A. V. Radyushkin, Phys. Rept. **418**, 1 (2005) [arXiv:hep-ph/0504030].
- [15] E. R. Berger, M. Diehl and B. Pire, Eur. Phys. J. C **23**, 675 (2002) [arXiv:hep-ph/0110062].
- [16] E. R. Berger, M. Diehl and B. Pire, Phys. Lett. B **523**, 265 (2001) [arXiv:hep-ph/0110080].
- [17] M. Diehl, T. Gousset and B. Pire, Phys. Rev. D **62**, 073014 (2000) [arXiv:hep-ph/0003233].
- [18] L. Mankiewicz, G. Piller and A. Radyushkin, Eur. Phys. J. C **10**, 307 (1999) [arXiv:hep-ph/9812467].
- [19] L. L. Frankfurt, P. V. Pobylitsa, M. V. Polyakov and M. Strikman, Phys. Rev. D **60**, 014010 (1999).
- [20] A. Airapetian *et al.* [HERMES Collaboration], Phys. Rev. Lett. **87**, 182001 (2001).
- [21] A. Airapetian *et al.* [HERMES Collaboration], Phys. Rev. D **75**, 011103 (2007).
- [22] Z. Ye [HERMES Collaboration], arXiv:hep-ex/0606061.
- [23] S. Stepanyan *et al.* [CLAS Collaboration], Phys. Rev. Lett. **87**, 182002 (2001).
- [24] C. Munoz Camacho *et al.* [Jefferson Lab Hall A Collaboration], Phys. Rev. Lett. **97**, 262002 (2006).
- [25] F. X. Girod *et al.* [CLAS Collaboration], arXiv:0711.4805 [hep-ph].
- [26] H. Fraas, B. J. Read and D. Schildknecht, Nucl. Phys. B **86**, 346 (1975).
- [27] P. Ditsas, B. J. Read and G. Shaw, Nucl. Phys. B **99**, 85 (1975).

- [28] G. Shaw, Phys. Rev. D **47**, 3676 (1993).
- [29] L. Frankfurt, V. Guzey and M. Strikman, Phys. Rev. D **58**, 094039 (1998).
- [30] S. Chekanov *et al.* [ZEUS Collaboration], Phys. Lett. B **573**, 46 (2003) [arXiv:hep-ex/0305028].
- [31] A. Aktas *et al.* [H1 Collaboration], Eur. Phys. J. C **44**, 1 (2005) [arXiv:hep-ex/0505061].
- [32] N. Kivel, M. V. Polyakov and M. Vanderhaeghen, Phys. Rev. D **63**, 114014 (2001).
- [33] A. Freund, Phys. Rev. D **68**, 096006 (2003).
- [34] A. V. Radyushkin and C. Weiss, Phys. Rev. D **63**, 114012 (2001).
- [35] L. Frankfurt, V. Guzey and M. Strikman, Phys. Rev. D **71**, 054001 (2005).
- [36] R. P. Feynman, *Photon-Hadron Interactions* (Benjamin, Reading, 1972).
- [37] T. H. Bauer, R. D. Spital, D. R. Yennie and F. M. Pipkin, Rev. Mod. Phys. **50**, 261 (1978)
[Erratum-ibid. **51**, 407 (1979)].
- [38] K. Fujikawa, Phys. Rev. D **4**, 2794 (1971).
- [39] V. N. Gribov, Sov. Phys. JETP **30** (1970) 709 [Zh. Eksp. Teor. Fiz. **57** (1969) 1306].
- [40] H. Fraas and D. Schildknecht, Phys. Lett. B **35**, 72 (1971).
- [41] A. Dar, Annals Phys. **65**, 324 (1971).
- [42] W. M. Yao *et al.* [Particle Data Group], J. Phys. G **33**, 1 (2006).
- [43] S. Aid *et al.* [H1 Collaboration], Nucl. Phys. B **463**, 3 (1996) [arXiv:hep-ex/9601004].
- [44] J. Breitweg *et al.* [ZEUS Collaboration], Eur. Phys. J. C **2**, 247 (1998) [arXiv:hep-ex/9712020].
- [45] C. Adloff *et al.* [H1 Collaboration], Eur. Phys. J. C **13**, 371 (2000) [arXiv:hep-ex/9902019].
- [46] A. Pautz and G. Shaw, Phys. Rev. C **57**, 2648 (1998) [arXiv:hep-ph/9710235].
- [47] S. Chekanov *et al.* [ZEUS Collaboration], Nucl. Phys. B **627**, 3 (2002) [arXiv:hep-ex/0202034].
- [48] V. N. Gribov and A. A. Migdal, Sov. J. Nucl. Phys. **8**, 583 (1969) [Yad. Fiz. **8**, 1002 (1968)].
- [49] L. Schoeffel, arXiv:0706.3488 [hep-ph].
- [50] A. Freund, M. McDermott and M. Strikman, Phys. Rev. D **67**, 036001 (2003).
- [51] L. N. Hand, Phys. Rev. **129**, 1834 (1963).
- [52] G. Piller and W. Weise, Phys. Rept. **330**, 1 (2000) [arXiv:hep-ph/9908230].
- [53] C. W. De Jager, H. De Vries and C. De Vries, Atom. Data Nucl. Data Tabl. **36**, 495 (1987).
- [54] A. Freund and M. Strikman, Phys. Rev. C **69**, 015203 (2004).